

Secular models and Kozai resonance for planets in coorbital non-coplanar motion

C. A. Giuppone^{1,2*}, A.M.Leiva¹

¹ *Universidad Nacional de Córdoba, Observatorio Astronómico, Laprida 854, X5000BGR Córdoba, Argentina*

² *Universidad Nacional de Córdoba, Observatorio Astronómico, IATE, Laprida 854, X5000BGR Córdoba, Argentina*

MNRAS accepted. Last updated 2016 April 27; in original form 2015 December 11

ABSTRACT

In this work, we construct and test an analytical and a semianalytical secular models for two planets locked in a coorbital non-coplanar motion, comparing some results with the case of restricted three body problem.

The analytical average model replicates the numerical N-body integrations, even for moderate eccentricities ($\lesssim 0.3$) and inclinations ($\lesssim 10^\circ$), except for the regions corresponding to quasi-satellite and Lidov-Kozai configurations. Furthermore, this model is also useful in the restricted three body problem, assuming very low mass ratio between the planets. We also describe a four-degree-of-freedom semianalytical model valid for any type of coorbital configuration in a wide range of eccentricities and inclinations.

Using a N-body integrator, we have found that the phase space of the General Three Body Problem is different to the restricted case for inclined systems, and establish the location of the Lidov-Kozai equilibrium configurations depending on mass ratio. We study the stability of periodic orbits in the inclined systems, and find that apart from the robust configurations L_4 , AL_4 , and QS is possible to harbour two Earth-like planets in orbits previously identified as unstable U and also in Euler L_3 configurations, with bounded chaos.

Key words: planets and satellites: dynamical evolution and stability, methods: analytical, celestial mechanics, Planetary systems.

1 INTRODUCTION

The three body problem has been studied since decades, particularly with more interest in the coorbital problem. The coorbital problem or 1:1 mean motion resonance (1:1 MMR) occurs when considering a central star and two planets. The period of the planets is almost the same, although the resonance acts avoiding collisions between the bodies. During the last years, several approaches were developed to find new types of regular orbits for this resonance and, in particular, surface of sections in parametric spaces (Hadjimetriou et al. 2009; Hadjimetriou & Voyatzis 2011), semi-analytical models (Giuppone et al. 2010), and analytical models (Robutel & Pousse 2013) were used.

Efforts have been made to determine the possibility of the detection of coorbital planets through the radial velocity signal (Giuppone et al. 2012; Dobrovolskis 2013; Leleu et al. 2015), transit detection (Ford & Gaudi 2006) or transit timing variations in the case that one or both planets transit

the stellar disc (Vokrouhlický & Nesvorný 2014; Haghighipour et al. 2013; Ford & Holman 2007). Although we still do not know details of dominant formation and evolutionary processes of these planetary systems, as well as their type, a general discussion has been established about whether or not the planets can be captured in the MMR 1:1.

Particularly, in non-coplanar case, we think that it is important to compare the general problem to the restricted problem because these results can be applied on our own Solar System. For example, the dynamical structure of the coorbital region provides a possible origin for coorbital satellites of the planets. As pointed by Namouni (1999) and Mikkola et al. (2006) transitions from Horseshoe or Tadpole orbits to quasi satellite orbits can be thought as a transport mechanism of distant coorbiting objects to a state of temporary or permanent capture around the planet. Once trapped, additional mechanisms provide subsequent permanent capture, for example, collisions with other satellites, mass growth of the planet and the drag of the circumplanetary nebula. This model can be useful even in the formation of the Janus-Epimetheus system through collisions. Re-

* E-mail: cristian@oac.unc.edu.ar

cently, [Morais & Namouni \(2016\)](#) showed that resonant capture in coorbital motion is present for both prograde and retrograde orbits.

Classical celestial mechanics books ([Brouwer & Clemence 1961](#); [Moulton 1914](#)) deal with Lagrangian equilibrium points and the orbits around them in the context of the Restricted Three Body Problem (RTBP): Horseshoe (HS) and Tadpole (TP) orbits. However, some other equilibrium orbits were identified, recently. As far as we know, three different kind of periodic orbits can be found in the averaged general three body problem. It is convenient to describe the configurations with two angles $(\sigma, \Delta\varpi) = (\lambda_2 - \lambda_1, \varpi_2 - \varpi_1)$, where λ_i are mean longitudes and ϖ_i are longitudes of pericentre of the planets. Apart from the well known equilateral configurations, located at the classical equilibrium Lagrangian points (L_4 and L_5) with angles $(\sigma, \Delta\varpi) = (\pm 60^\circ, \pm 60^\circ)$, Quasi-Satellite (QS) orbits and Anti-Lagrangian orbits (AL_4 and AL_5) are present. For low eccentricities, Anti-Lagrangian orbits are located at $(\sigma, \Delta\varpi) = (\pm 60^\circ, \mp 120^\circ)$. One anti-Lagrangian solution AL_i is connected to the corresponding L_i solution through the σ -family of periodic orbits in the averaged system (the solutions with zero-amplitudes of the σ -oscillation). The QS orbits are characterized by oscillations around a fixed point, which is always located at $(\sigma, \Delta\varpi) = (0^\circ, 180^\circ)$, independently on the planetary mass ratio and eccentricities. In the top right-hand panel of Figure 1, we construct a dynamical map with a grey scale indicating the amplitude of oscillation of σ on the plane $(\sigma, \Delta\varpi)$ identifying the equilibrium orbits. Each of the other plots shows the orbital representation of some configurations in (x, y) astrometric Cartesian coordinates. We focus our attention on L_4 and AL_4 configurations, because L_5 and AL_5 configurations are dynamically equivalent to the formers (see [Giuppone et al. 2010](#); [Hadjidemetriou et al. 2009](#)). Additionally, in the Figure 1 we marked with light circles the location of Euler configuration, L_3 , and the center of unstable family U studied by [Hadjidemetriou et al. \(2009\)](#) and afterwards related with the L_3 configuration by [Robutel & Pousse \(2013\)](#). We pay special attention to both configurations at the final section. Note that L_3 is located at $(\sigma, \Delta\varpi) = (180^\circ, 180^\circ)$, while unstable configuration U is located at $(\sigma, \Delta\varpi) = (180^\circ, 0^\circ)$.

In Section 2 we present the Hamiltonian analytical model with elliptic expansions and explore the validity of the average model. Also, we compare the results with direct N-body integrations. In Section 3 we introduce the average semianalytical model for the three-body problem in non-coplanar case, extending previous results, and compare to numerically filtered integrations. Following, in Section 4, we focus on the study of 3D equilibrium orbits, particularly on the Lidov-Kozai resonance with the different models. Finally, conclusions are presented in Section 5.

2 ANALYTICAL MODEL

Classical expansions of the disturbing function do not converge when the semi-major axis ratio is $\simeq 1$, and consequently they are not appropriate to model the coorbital resonance. Then, our intention is to give an easy handle Hamiltonian to describe the motion within this resonance. We consider a system of two planets with masses m_i moving

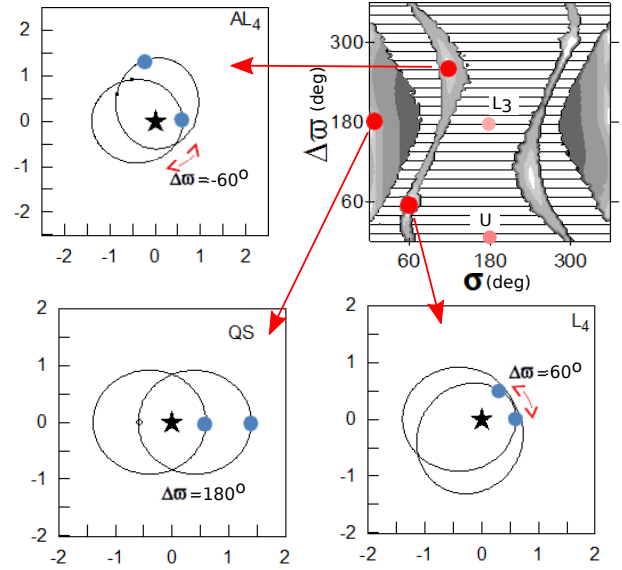


Figure 1. Top right-hand panel shows a dynamical map on the plane $(\sigma, \Delta\varpi)$ with the colour scale representing the oscillation amplitude of σ . Initial osculating elements correspond to two Jupiter planets orbiting a $1 M_\odot$ star at 1 au with initial osculating eccentricities $e_i = 0.4$. The gray scale indicates the amplitude of oscillation for σ and the dashed region corresponds to unstable configurations. In the remaining panels we identify the three periodic orbits QS , L_4 and AL_4 and plot their representation in the plane (x, y) with the star at the origin. Initial conditions for both planets are shown with blue circles, with m_1 located along the x -axis. Both axis directions are fixed.

around a star with mass m_0 with inclinations lower than 90° . We not include additional planets neither dissipative forces. Each planetary orbit is described by six orbital elements: semi-major axis a , eccentricity e , inclination i , longitude of pericentre ϖ , mean longitude in orbit λ , and longitude of the node Ω . Alternatively we can use the argument of pericentre $\omega = \varpi - \Omega$, mean anomaly $M = \lambda - \varpi$, and true anomaly f .

We write the Hamiltonian following [Laskar & Robutel \(1995\)](#), using a canonical set of variables introduced by Poincaré with astrometric positions of the planets \mathbf{r}_i , and barycentric momentum vectors \mathbf{p}_i . The pairs $(\mathbf{r}_i, \mathbf{p}_i)$ form a canonical set of variables with the Hamiltonian given by

$$H = H_0 + U + T \quad (1)$$

Here, H_0 is the Keplerian part (sum of the independent Keplerian Hamiltonians), U is the direct part, and T is the kinetic part of the Hamiltonian, written in terms of the canonical variables $(\mathbf{r}_i, \mathbf{p}_i)$ as

$$\begin{aligned} H_0 &= - \sum_{i=1}^N \left(\frac{p_i^2}{2\beta_i} - \frac{m_0 m_i}{|\mathbf{r}_i|} \right), \\ U &= - \mathcal{G} \sum_{i,j=1}^N \frac{m_i m_j}{\Delta_{ij}}, \\ T &= \sum_{i,j=1}^N \frac{\mathbf{p}_i \cdot \mathbf{p}_j}{m_0}, \end{aligned} \quad (2)$$

where \mathcal{G} is the gravitational constant, $\beta_i = m_0 m_i / (m_0 + m_i)$ and $\Delta_{ij} = \|\mathbf{r}_i - \mathbf{r}_j\|$.

In the three-body problem, the barycentric momenta, \mathbf{p}_i , are related to the heliocentric velocities, $\dot{\mathbf{r}}_i$, by the following expressions

$$\begin{aligned} \mathbf{p}_1 &= \frac{m_1}{m_0 + m_1 + m_2} [(m_0 + m_2)\dot{\mathbf{r}}_1 - m_2\dot{\mathbf{r}}_2], \\ \mathbf{p}_2 &= \frac{m_2}{m_0 + m_1 + m_2} [(m_0 + m_1)\dot{\mathbf{r}}_2 - m_1\dot{\mathbf{r}}_1]. \end{aligned} \quad (3)$$

For the planetary case $m_i \ll m_0$, then

$$\begin{aligned} \mathbf{p}_1 &\simeq m_1\dot{\mathbf{r}}_1 + \frac{m_1 m_2}{m_0} (\dot{\mathbf{r}}_1 - \dot{\mathbf{r}}_2) \\ \mathbf{p}_2 &\simeq m_2\dot{\mathbf{r}}_2 + \frac{m_1 m_2}{m_0} (\dot{\mathbf{r}}_2 - \dot{\mathbf{r}}_1). \end{aligned} \quad (4)$$

The distance, Δ , between the planets is

$$\Delta^2 = r_1^2 + r_2^2 - 2r_1 r_2 \cos \phi \quad (5)$$

being ϕ , the angle between the vectors \mathbf{r}_1 and \mathbf{r}_2 ,

$$\cos \phi = \frac{\mathbf{r}_1 \cdot \mathbf{r}_2}{r_1 r_2} \quad (6)$$

We then expand positions and velocities in eccentricities, e_j , and inclinations, $s_j = \sin(i_j/2)$, obtaining an analytic expansion for the Hamiltonian \mathcal{H} . Also, we keep the coefficients up to the order $\mathcal{O}(e_j^2)$, $\mathcal{O}(s_j^2)$, and $\mathcal{O}(m_j)$. Then, we integrate over the fast angle $\lambda_1 + \lambda_2$, recovering the averaged analytical Hamiltonian \mathcal{H}_2 as

$$\begin{aligned} \mathcal{H}_2 &= \mathcal{H}_{00} + \mathcal{G} m_1 m_2 \mathcal{H}_{22}, \\ \mathcal{H}_{00} &= -\frac{\beta_1 \mu_1}{2a_1} - \frac{\beta_2 \mu_2}{2a_2} + \mathcal{G} m_1 m_2 \left(\frac{\cos \sigma}{\sqrt{a_1 a_2}} - \frac{1}{\Delta} \right), \\ \mathcal{H}_{22} &= H_{2000} (e_1^2 + e_2^2) + H_{1100} e_1 e_2 \\ &\quad + H_{0020} (s_1^2 + s_2^2) + H_{0011} s_1 s_2, \end{aligned} \quad (7)$$

where

$$\begin{aligned} \mu_i &= \mathcal{G}(m_0 + m_i), \\ \sigma &= \lambda_2 - \lambda_1, \\ \tilde{\Delta} &= \sqrt{a_1^2 + a_2^2 - 2a_1 a_2 \cos(\sigma)}, \end{aligned} \quad (8)$$

\mathcal{H}_{00} has zero-order terms in eccentricities and inclinations, and \mathcal{H}_{22} has order two terms, formally:

$$\begin{aligned} H_{2000} &= -\frac{\cos(\sigma)}{2\sqrt{a_1 a_2}} \\ &\quad + \frac{a_1 a_2}{8\tilde{\Delta}^5} [4\cos(\sigma)(a_1^2 + a_2^2) + a_1 a_2 (5\cos(2\sigma) - 13)], \\ H_{1100} &= \frac{\cos(\Delta\varpi - 2\sigma)}{\sqrt{a_1 a_2}} + \frac{\gamma}{\tilde{\Delta}^5}, \\ \gamma &= -a_1 a_2 (a_1^2 + a_2^2) \cos(\Delta\varpi - 2\sigma) - \frac{a_1^2 a_2^2}{8} \\ &\quad [\cos(\Delta\varpi - 3\sigma) - 26\cos(\Delta\varpi - \sigma) + 9\cos(\Delta\varpi + \sigma)], \\ H_{0020} &= \left(\frac{a_1 a_2}{\tilde{\Delta}^3} - \frac{1}{\sqrt{a_1 a_2}} \right) \cos(\sigma) \\ H_{0011} &= 2 \left(\frac{1}{\sqrt{a_1 a_2}} - \frac{a_1 a_2}{\tilde{\Delta}^3} \right) \cos(\Omega_2 - \Omega_1 - \sigma). \end{aligned} \quad (9)$$

This expression for \mathcal{H}_2 is equivalent to the one reported in

Robutel & Pousse (2013), but avoiding the Complex notation. We also want to remark that, due to the D'Alembert rules only even powers of eccentricities and inclinations are present in \mathcal{H}_2 .

The first-order average Hamiltonian, given by the expression \mathcal{H}_2 , is not valid in the region of QS because the fast angle $(\lambda_1 + \lambda_2)$ has a similar period to that of the resonant one (σ) ¹.

The integrable approximation \mathcal{H}_{00} , associated to the circular and planar resonant problem, was used by some authors to study the motion inside the resonance because it should provide qualitative information about the system dynamics. However, this approximation is inadequate to describe the real dynamics of the planets, even in some simple cases. We put in evidence this fact comparing the integrations projected in the plane (u, σ) , using the analytic expansion \mathcal{H} with the results from the integrable approximation \mathcal{H}_{00} ; being

$$u = \frac{\sqrt{\mu_1 \mu_2}}{\sqrt{\mathcal{G} m_0}} \frac{\beta_1 \beta_2}{(\beta_1 + \beta_2)} \frac{(\sqrt{a_1} - \sqrt{a_2})}{(\beta_1 \sqrt{\mu_1 a_1} + \beta_2 \sqrt{\mu_2 a_2})} \quad (10)$$

the dimensionless non canonical action-like variable.

In Figure 2 we compare the evolution of initial conditions in the plane (σ, u) using the integrable approximation \mathcal{H}_{00} , the analytical expansion \mathcal{H} , and N-body simulations. From left to right initial conditions corresponds to two Jupiter-like planets in coplanar quasi circular orbits ($e_i = 0.01$), in eccentric orbits ($e_i = 0.15$), and two Earth-like planets in eccentric orbits ($e_i = 0.15$). Initial conditions are set for $\sigma = 2^\circ, 60^\circ, 180^\circ$, and 300° for different u values around zero. Consequently, the semi-major axes are

$$a_i = \bar{a} \left(1 + (-1)^{i+1} \frac{\beta_1 + \beta_2}{\beta_j} \sqrt{\frac{\mu_0}{\mu_j}} u \right)^2 \quad (11)$$

were the parameter \bar{a} is the mean value around which the semi-major axes oscillate, $\bar{a} = 1$ (see Robutel & Pousse 2013). Also, the initial conditions for $\Delta\varpi$ are set according to the nearest value of the equilibrium solutions, namely $\sigma \simeq 0^\circ \rightarrow \Delta\varpi = 180^\circ$, and $\sigma \simeq \pm 60^\circ \rightarrow \Delta\varpi = \pm 60^\circ$. The top row shows integrations given by the analytical \mathcal{H} (red dots) and \mathcal{H}_{00} (green lines), while the bottom row shows the same initial conditions, but integrated with a full N-body code. Strictly speaking, our figures depict a projection of the orbital elements on the phase-space portraits. In order to draw a formal parallel between numerically computed phase-space portraits and their analytic counterparts, a numerical averaging process must be appropriately carried out over the rapidly varying angles. However, for the purposes of this work, we shall loosely refer to these plots as phase-space portraits, since their information content is almost identical.

At bottom Frame of Figure 2 we can see that for Jupiter-like planets only small-amplitude Tadpole orbits are stable. The remaining conditions are highly unstable (can be seen as sparsely points) and neither QS nor HS exist for more than a few orbits. Then, we set a threshold to stop the integrations when the mutual distance between bodies is smaller than the sum of their mutual radius (assuming Earth or Jupiter radius, depending on the case) or if they

¹ Recently, Robutel et al. (2015) have proposed a valid rigorous average method in this region.

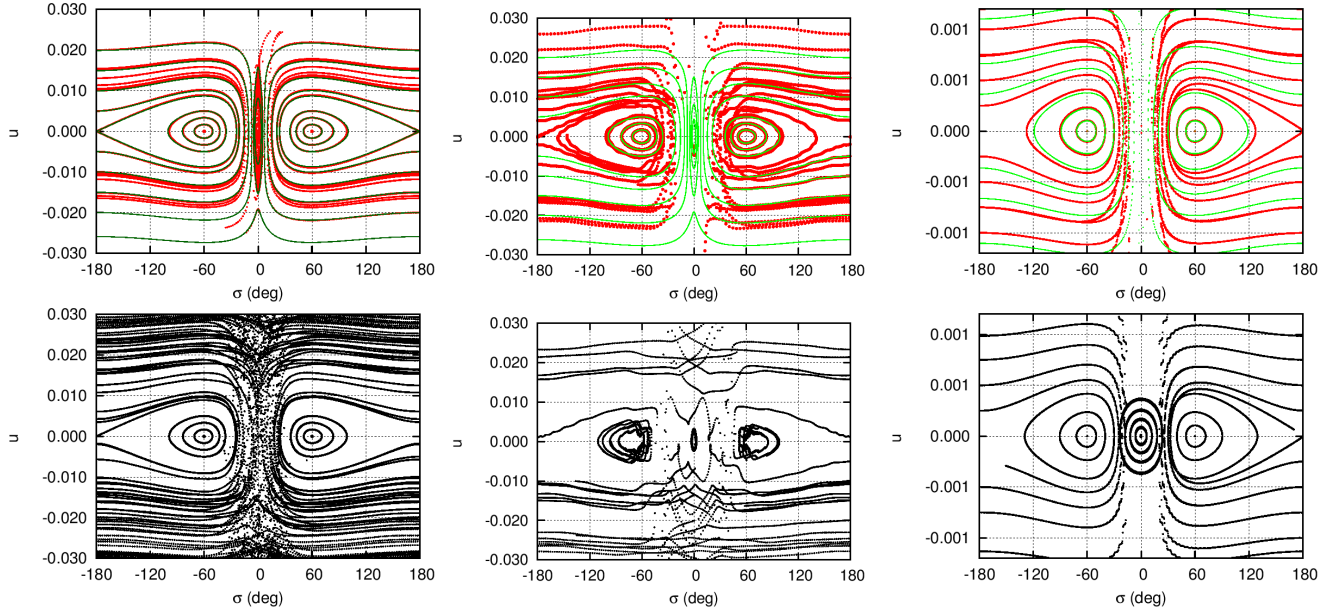


Figure 2. Top row. Phase space described by initial conditions integrated using \mathcal{H} and \mathcal{H}_{00} in the plane (u, σ) . Jupiter-like planets in quasi circular orbits (left panel), Jupiter-like planets in eccentric orbits (middle panel) and Earth-like planets in eccentric orbits (right panel). Bottom-row. The same initial conditions integrated with the N-body code for 400 years. See text for details.

exhibit a chaotic behaviour changing their configuration. We also find transitions from *HS* or Tadpole orbits to *QS* orbits. Moreover, for quasi circular orbits ($e_i = 0.01$), it is evident that the integrable approximation (top row) \mathcal{H}_{00} is not good to describe the real dynamics, and that the inclusion of lower-order terms of eccentricities present in \mathcal{H} are enough to destabilise the system. Furthermore, only Tadpoles orbits around L_4 and L_5 remain stable (top left and middle panels of Fig 2). At right-hand panel of Fig 2, with moderate initial eccentricities but planetary masses very small, $m_i/m_0 = 3 \times 10^{-6}$, the dynamics predicted by the integrable approximation \mathcal{H}_{00} are similar to \mathcal{H} ; however, the *QS* region is only present in the N-body integrations (bottom right panel).

To understand what happen in *HS* configuration, the Figure 3 shows an example of variation of u with time, integrated with different models, for a Jupiter pair of planets. The inclusion of eccentric terms is responsible for instability, even if the initial conditions belong to quasi circular orbits ($e_i = 0.01$).

To study the *HS* configuration we use the results from Robutel & Pousse (2013), that estimated the size of *HS* (U_1) and *TP* (U_3) region as:

$$U_1 = \frac{3^{1/6}}{2^{1/3}} \frac{m_1 m_2}{m_0^{1/3} (m_1 + m_2)^{5/3}}$$

$$U_3 = \frac{2^{1/2}}{3^{1/2}} \frac{m_1 m_2}{m_0^{1/2} (m_1 + m_2)^{3/2}}$$

$$\frac{U_1}{U_3} = \frac{3^{2/3}}{2^{5/6}} \left(\frac{m_0}{m_1 + m_2} \right)^{1/6}. \quad (12)$$

Thus, the ratio $\frac{U_1}{U_3}$ give us the size of the *HS* region relative to the *TP* region. As masses decrease, the relative size increases, but the absolute size is more reduced.

Laughlin & Chambers (2002) mentioned that the *HS*

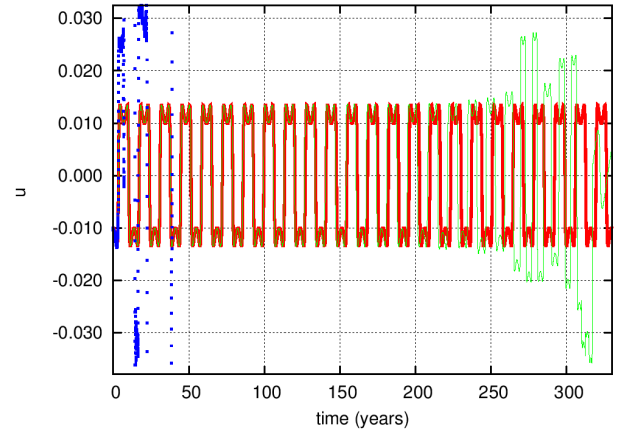


Figure 3. Evolution of u for a coplanar Horseshoe pair of Jupiter planets with initial condition at $(u, \sigma) = (-0.01, 180^\circ)$, using \mathcal{H}_{00} (thick red line), \mathcal{H} (green line) and N-body integrations (blue dots). The inclusion of lower order terms of the eccentricities rapidly excites the system causing the disruption of the resonance (time $\simeq 250$ periods). The N-body simulation rapidly evidences the chaotic nature of this configuration (time $\simeq 5$ periods).

configuration is not stable for planets more massive than $0.4M_J$ ($\sim 100 M_\oplus$) for quasi circular orbits ($e_i = 0.01$). Recently, Leleu et al. (2015) have shown that the *HS* configuration is stable for systems with masses lower than $\sim 30 M_\oplus$ ($e_i = 0.05$). Thus, Setting the initial conditions very close to the value of U_3 ($1.2 U_3$) we numerically integrate the three-body problem for different masses ($m_1 = m_2$) and initial eccentricities ($e_1 = e_2$), and calculate their Mean Exponential Growth factor of Nearby Orbits $\langle Y \rangle$ to analyse their chaoticity (i.e. MEGNO, Cincotta & Simó 2000). Figure 4 shows the values of $\langle Y \rangle$ for 5×10^4 periods for coplanar or-

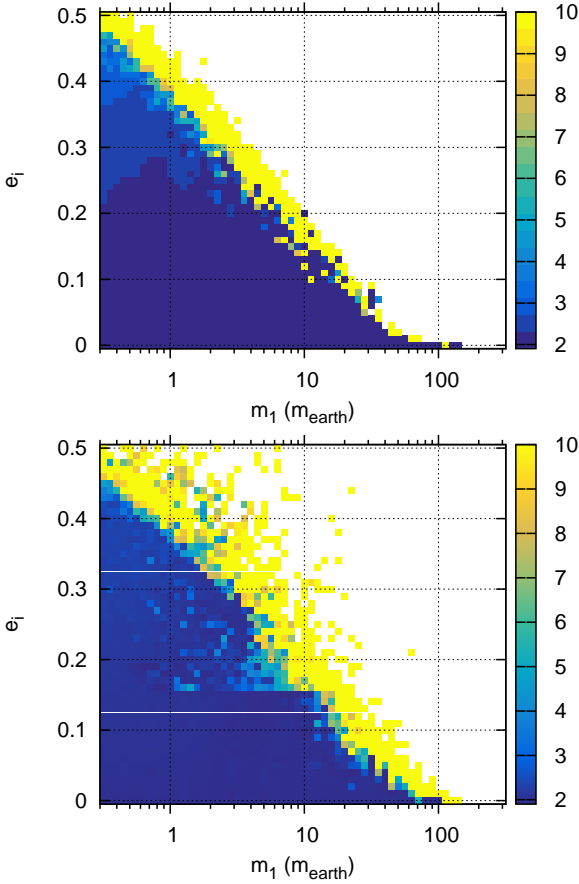


Figure 4. Stability of *HS* orbits in the plane of osculating initial conditions (m_1, e_i) with $(\sigma, \Delta\varpi) = (60^\circ, 60^\circ)$. Semi-major axis initial values are taken from Eq.11, setting $u = 1.2U_3$. The colour code indicates the value of $\langle Y \rangle$. Strongly chaotic systems or systems that quit the coorbital resonance before the integration stops are marked with white dots. All coloured orbits survive for at least 10^5 periods. Long term integrations show that slow chaotic orbits ($\langle Y \rangle \gtrsim 5$) survive from 5×10^5 to 8×10^6 periods, while unstable conditions (in white) not survive for more than 2×10^3 periods. Initial conditions correspond to coplanar configurations (top panel), and initial mutual inclinations $J = 15^\circ$ (bottom panel).

bits ($J = 0^\circ$) and initially mutual inclined orbits ($J = 15^\circ$)². In the figure, we can identify the allowed maximum mass values in function of their initial eccentricities for *HS* planets. These values agree with other authors results regarding to coplanar orbits. We run long-term numerical simulations (10 Myr) for selected initial conditions (specially for $e_i > 0.3$) and the initial conditions with $\langle Y \rangle \gtrsim 5$ did not survive, maybe due to the long-term diffusion that destabilize the coorbital systems on a time scale that varies from 5×10^5 to 8×10^6 periods (see Páez & Efthymiopoulos 2015). Gen-

² When both planets have masses, it is convenient to work with mutual inclination J , defined as $\cos J = \cos i_1 \cos i_2 + \sin i_1 \sin i_2 \cos(\Omega_1 - \Omega_2)$ (deduced from spherical trigonometry, see Moulton 1914, pg. 408).

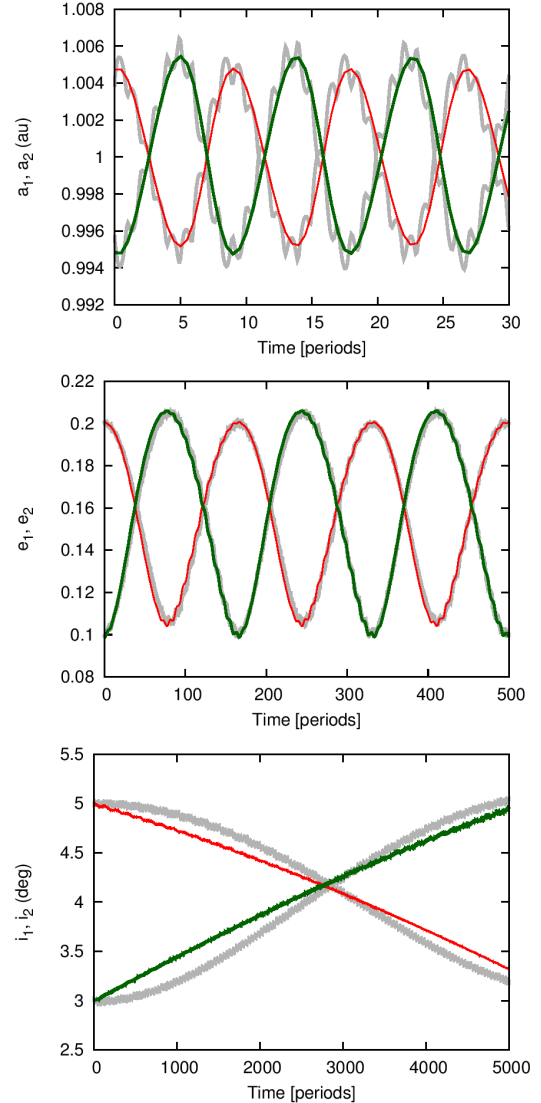


Figure 5. Variation of orbital elements with time using the analytical \mathcal{H}_2 model compared with a N-body integration. Amplitudes coincide perfectly and the frequencies were adjusted by hand (see text). Initial conditions from Table 1 for the L_4 case.

erally, the inclined systems ($J = 15^\circ$) can survive for more periods; however, they are strongly chaotic, and those orbits with $e_i \gtrsim 0.15$ are frequently transition orbits (*HS* – *QS*).

We have tested the second-order averaged Hamiltonian, \mathcal{H}_2 , setting the initial conditions near equilibrium configurations with moderate eccentricities ($e_j < 0.3$) and mutual inclinations ($J < 12^\circ$). Moreover, the mean initial Poincaré orbital elements were calculated using a low pass FIR digital filter (Carpino et al. 1987) to eliminate all periodic variations with a period smaller than 3 years. We have selected initial conditions from Table 1 to illustrate the orbital evolution, and the results are shown in Figures 5, 6, and 7. We can see a perfect agreement between the N-body integration and the \mathcal{H}_2 model for L_4 , AL_4 , and the *HS* configurations respectively. We resolve the Hamiltonian equations using 5 and 6 degrees of freedom, i.e. equations (13) and (14), and the results are the same.

We must remark that the integrations with the \mathcal{H}_2

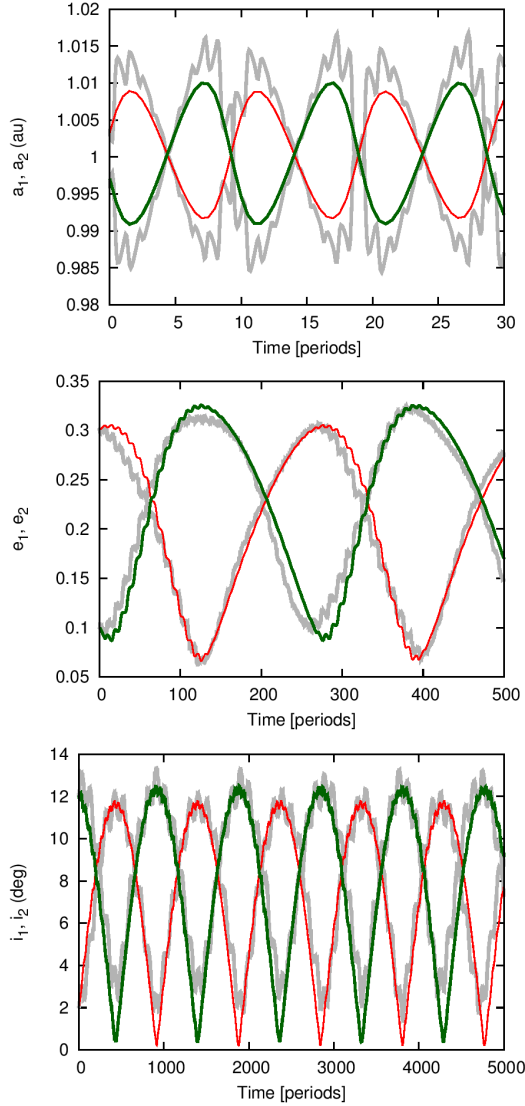


Figure 6. Variation of orbital elements with time using the analytical \mathcal{H}_2 model compared with a N-body integration. Initial conditions from Table 1 correspond to the AL_4 case.

model modify the period of the orbital elements. As a consequence, the secular frequencies sometimes depend on the initial values of e and i . Thus, except for very small e and i , the secular frequencies are poorly approximated, which is a problem for the study of the resonances (inside the coorbital resonance), and especially the Lidov-Kozai resonance. For the initial conditions chosen for Figures 5, 6 & 7, the periods of the eccentricities are 20% longer than those determined with the N-body integrations. When we modify the initial inclinations, the periods can be even four times the real ones. To show this, in top panel of Figure 8 we show the secular periods calculated with \mathcal{H}_2 and N-body filtered integrations varying the initial eccentricities and two different initial mutual inclinations ($J = 0^\circ$ and $J = 15^\circ$), while in bottom panel we set the initial eccentricities at $e_1 = e_2 = 0.01$ and $e_1 = e_2 = 0.15$ for different mutual inclinations. The secular frequencies almost do not depend on the initial values of e in the N-body integrations. For near circular orbits and planar orbits the secular frequencies are well approximated by \mathcal{H}_2 . When the eccentricity increases the frequencies are

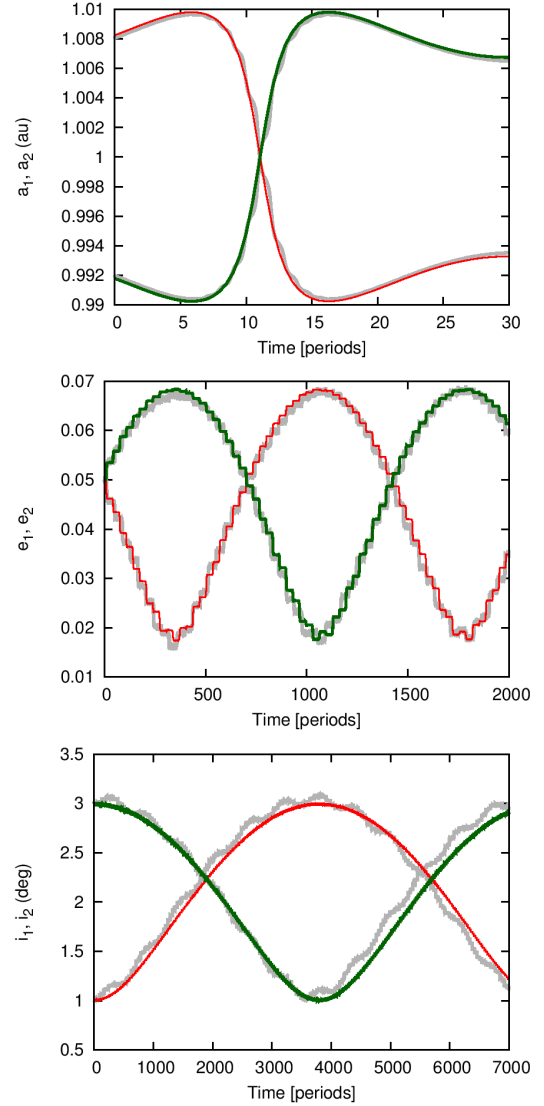


Figure 7. Variation of orbital elements with time using the analytical \mathcal{H}_2 model compared with a N-body integration. Initial conditions from Table 1 correspond to the HS case.

	σ	$\Delta\varpi$	e_1	e_2	i_1	i_2
L_4	60	60	0.2	0.1	5	3
AL_4	60	240	0.3	0.1	2	12
HS	240	240	0.05	0.05	1	3
QS	0	180	0.45	0.45	1	3

Table 1. Osculating Poincaré initial conditions near the stable periodic solutions in the $(\sigma, \Delta\varpi)$ plane. All conditions have all angles in degrees, $m_1 = 1M_J$, $m_2 = 0.9M_J$, $a_1 = 1.0038$ au, and $a_2 = 0.995784$ au. HS has $u = 0.002$ and masses $m_i = 12.5M_\oplus$.

poorly determined by the \mathcal{H}_2 model. On the contrary, when we fixed the initial eccentricities at $e = 0.01$ for different mutual inclinations, neither the N-body simulations nor the \mathcal{H}_2 model have constant secular frequencies (bottom panel of Figure 8).

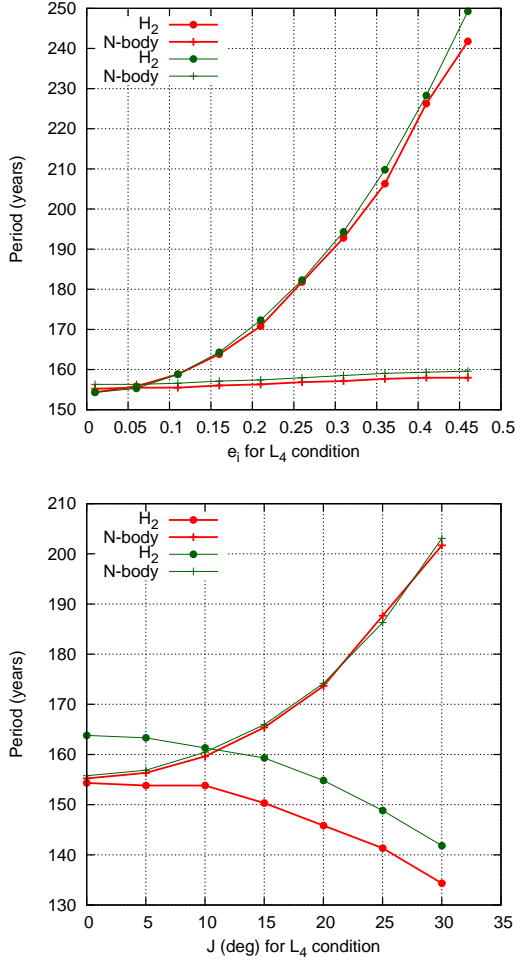


Figure 8. Secular period calculated using the H_2 model (circles) compared with the N-body integration (crosses). Initial osculating angles correspond to the L_4 configuration. Top panel. Thick lines have coplanar initial conditions, while thin lines have initial value $J = 15^\circ$. Bottom panel. Thick lines have quasi circular initial conditions ($e_i = 0.01$), while thin lines have initial values $e_i = 0.15$.

3 SEMIANALYTICAL MODEL

In order to extend the study of the system to the whole parameter space (e.g. planetary masses, eccentricities, inclinations, etc.), it is useful to construct a semi-analytical model for the coorbital motion. We followed the ideas for the 3D models in other resonances (e.g. [Beaugé & Michtchenko 2003](#)) extending the study of coplanar coorbital model developed in [Giuppone et al. \(2010\)](#).

Our model involves two main steps: first, a transformation to adequate resonant variables; second, a numerical averaging of the Hamiltonian with respect to short-period terms. Both procedures are detailed below.

We begin introducing the usual mass-weighted Poincaré canonical variables (e.g. [Laskar 1990](#)) for each planet with

mass m_i :

$$\begin{aligned} \lambda_1 &; L_1 = \beta_1 \sqrt{\mu_1 a_1} \\ \lambda_2 &; L_2 = \beta_2 \sqrt{\mu_2 a_2} \\ p_1 &= -\varpi_1 ; P_1 = L_1 - G_1 = L_1 \left(1 - \sqrt{1 - e_1^2}\right) \\ p_2 &= -\varpi_2 ; P_2 = L_2 - G_2 = L_2 \left(1 - \sqrt{1 - e_2^2}\right) \\ q_1 &= -\Omega_1 ; Q_1 = G_1 - H_1 \\ q_2 &= -\Omega_2 ; Q_2 = G_2 - H_2 \end{aligned} \quad (13)$$

where $\mu_i = \mathcal{G}(m_0 + m_i)$, $G_i = L_i \sqrt{1 - e_i^2}$, and $H_i = G_i \cos(i_i)$.

For the initial conditions in the vicinity of coorbital motion, we define the following set of resonant canonical variables $(R_1, R_2, S_1, S_2, T_1, T_2, \sigma, \Delta\varpi, s_1, s_2, t_1, t_2)$, where the new angles and actions are

$$\begin{aligned} \sigma &= \lambda_2 - \lambda_1 & R_1 &= \frac{1}{2}(L_2 - L_1) \\ \Delta\varpi &= p_1 - p_2 & R_2 &= \frac{1}{2}(P_1 - P_2) \\ s_1 &= \lambda_1 + \lambda_2 + p_1 + p_2 & S_1 &= \frac{1}{2}(L_1 + L_2) \\ s_2 &= -(p_1 + p_2) + (q_1 + q_2) & S_2 &= \frac{1}{2}(L_1 + L_2 - P_1 - P_2) \\ t_1 &= q_1 - q_2 & T_1 &= \frac{1}{2}(Q_1 - Q_2) \\ t_2 &= -(q_1 + q_2) & T_2 &= \frac{1}{2}(H_1 + H_2) \end{aligned} \quad (14)$$

given that

$$a_1 = \frac{(S_1 - R_1)^2}{\mu_1 \beta_1^2} \quad a_2 = \frac{(S_1 + R_1)^2}{\mu_2 \beta_2^2} \quad (15)$$

As we know, a generic argument, φ , of the disturbing function can be written as:

$$\varphi = j_1 \lambda_1 + j_2 \lambda_2 + j_3 \varpi_1 + j_4 \varpi_2 + j_5 \Omega_1 + j_6 \Omega_2, \quad (16)$$

where j_k are integers. In terms of the new angles, the same argument may be written as:

$$2\varphi = (j_2 - j_1)\sigma + (j_4 - j_3)\Delta\varpi + (j_1 + j_2)s_1 + \left(\sum_{k=1}^4 j_k\right)s_2 + (j_6 - j_5)t_1 + \left(\sum_{k=1}^6 j_k\right)t_2. \quad (17)$$

Since D'Alembert's relation provides a restriction for the j_k coefficients, $\sum_k j_k = 0$, t_2 does not appear in φ (t_2 is a cyclic angle). As a consequence, the associated action T_2 is a constant of motion and we can reduce our problem by one degree of freedom. Hence, our election of canonical variables leads to $T_2 = \frac{1}{2}(H_1 + H_2) = \frac{1}{2}\mathcal{AM}$ (half the orbital Angular Momentum of the system).

Then, the Hamiltonian function can be expressed as $\mathcal{H} = \mathcal{H}_0 + \mathcal{H}_1$, where \mathcal{H}_0 corresponds to the two-body contribution,

$$\mathcal{H}_0 = -\frac{\mu_1^2 \beta_1^3}{2L_1^2} - \frac{\mu_2^2 \beta_2^3}{2L_2^2}. \quad (18)$$

The second term, \mathcal{H}_1 , is the disturbing function which can be written as:

$$\mathcal{H}_1 = -\mathcal{G}m_1 m_2 \frac{1}{\Delta} + \mathcal{T}_1, \quad (19)$$

where Δ is the instantaneous distance between the two planets, and \mathcal{T}_1 is the indirect part of the potential energy of the gravitational interaction.

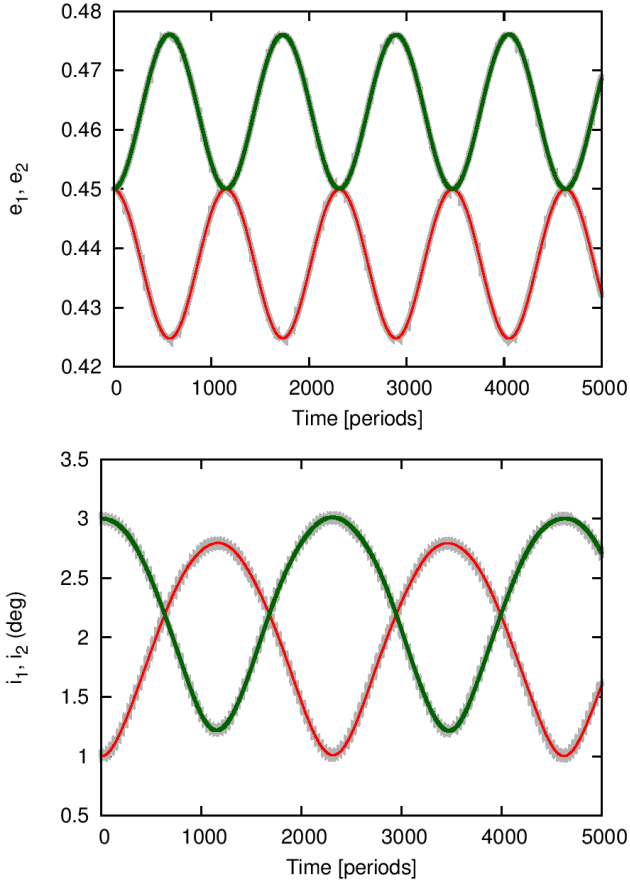


Figure 9. Time variation of eccentricities and inclinations using the semianalytical model, $\bar{\mathcal{H}}$, compared with a filtered N-body integration for the QS condition from Table 1.

Obviously, the equations 13 and 14 achieve the same results, but the latter has only 5-degrees-of-freedom, imposing the conservation of the angular momentum.

The next step is average of the Hamiltonian over the fast angle s_1 . This procedure can be performed numerically, allowing us to evaluate the averaged Hamiltonian $\bar{\mathcal{H}}$ as:

$$\bar{\mathcal{H}}(R_1, R_2, S_2, T_1, \sigma, \Delta\varpi, s_2, t_1; S_1, \mathcal{AM}) \equiv \frac{1}{4\pi} \int_0^{4\pi} \mathcal{H} ds_1. \quad (20)$$

In the averaged variables, S_1 is a new integral of motion which, in analogy to other mean-motion resonances, we identify as the *scaling parameter*, i.e. \mathcal{K} .

$\bar{\mathcal{H}}$ constitutes a system with four degrees of freedom in the canonical variables $(R_1, R_2, S_2, T_1, \sigma, \Delta\varpi, s_2, t_1)$, parametrized by the values of both \mathcal{K} and \mathcal{AM} . Since the numerical integration depicted in equation (20) is equivalent to a first-order average of the Hamiltonian function (e.g. Ferraz-Mello 2007), only those periodic terms with $j_1 + j_2 = 0$ remain in $\bar{\mathcal{H}}$ (see Eq. 17).

We have compared the semianalytical model averaged over the fast angle with the filtered N-body integrations. The filter was made using a low pass FIR digital filter (Carpino et al. 1987) to eliminate all periodic variations with a period smaller than 3 years. Needless to say, these results match better than those reproduced by the second order

Hamiltonian, \mathcal{H}_2 , but much slower. Due to the fact that we do not have restrictions for any configuration, $\bar{\mathcal{H}}$ is more adequate in the whole coorbital resonance. As an example, we show the results for an initial condition corresponding to a QS orbit in Figure 9. No significant differences are appreciated for actions, angles, frequencies neither for orbital elements.

Moreover, combining the information from Eq. 13 with the expansions in Eq. 9 we easily identify S_1, S_2 and T_2 as constants of motion. Thus, we can deduce the coupling in the orbital elements in the averaged models, namely

$$\begin{aligned} \beta_1 \sqrt{\mu_1 a_1} + \beta_2 \sqrt{\mu_2 a_2} &= \text{const} \\ L_1 e_1^2 + L_2 e_2^2 &\simeq \text{const} \end{aligned} \quad (21)$$

$$L_1 e_1^2 \cos(i_1) + L_2 e_2^2 \cos(i_2) \simeq \text{const}$$

From previous equations, the coupling between e and i present in the Lidov-Kozai resonance is not obvious (see Section 4).

We explore the parameter space $(\sigma, \Delta\varpi)$ and plot the relative difference between the mean Hamiltonian, $\bar{\mathcal{H}}$, and the average \mathcal{H}_2 model. The QS region³ shows more discrepancy, even considering Neptune-like planets in quasi circular orbits. In the Figure 10 we construct a colour map in the plane $(\sigma, \Delta\varpi)$ considering two Jupiter-like planets with quasi circular initial conditions, $e_i = 0.01$, and in eccentric orbits, $e_i = 0.15$. Also, we identify the initial mutual inclination, J , in each panel. Outside the QS region, the relative difference between Hamiltonians does not exceed 10^{-14} , justifying the region of validity for the \mathcal{H}_2 model. Furthermore, Analytical models valid for the QS or “eccentric retrograde satellite orbits”, were developed by Mikkola et al. (2006) and Sidorenko et al. (2014), but are only valid in the frame of the RTBP, considering small inclinations.

To illustrate the validity of this semianalytical model Figure 11 shows the integrations for the same initial conditions of Figure 2. Obviously, if the mutual inclination, J , or eccentricities, e_i , increases, the analytical Hamiltonian \mathcal{H}_2 is more inexact. The semianalytical model eliminates the short periodic terms and, is which is easier to identify the different types of motion.

4 PHASE SPACE IN THE 3D CASE

Our intention in this section is to find the different types of stable orbits present in the inclined systems for the 1:1 MMR.

Voyatzis et al. (2014) studied systems that migrate under the influence of dissipative forces that mimic the effects of gas-driven (Type II) migration. They demonstrated that sometimes excitation of inclinations occurs during the initial stages of planetary migration. In these cases, *vertical critical orbits* may generate stable families of 3D periodic orbits, which drive the evolution of the migrating planets to non-coplanar motion. Their work focuses on the calculus of the vertical critical orbits of the 2:1 and 3:1 MMR, for several values of the planetary mass ratio. In hierarchical systems,

³ The region defined around $(\sigma, \Delta\varpi) = (0^\circ, 180^\circ)$. See Giuppone et al. (2010) to identify the regions of motion within coorbital resonance.

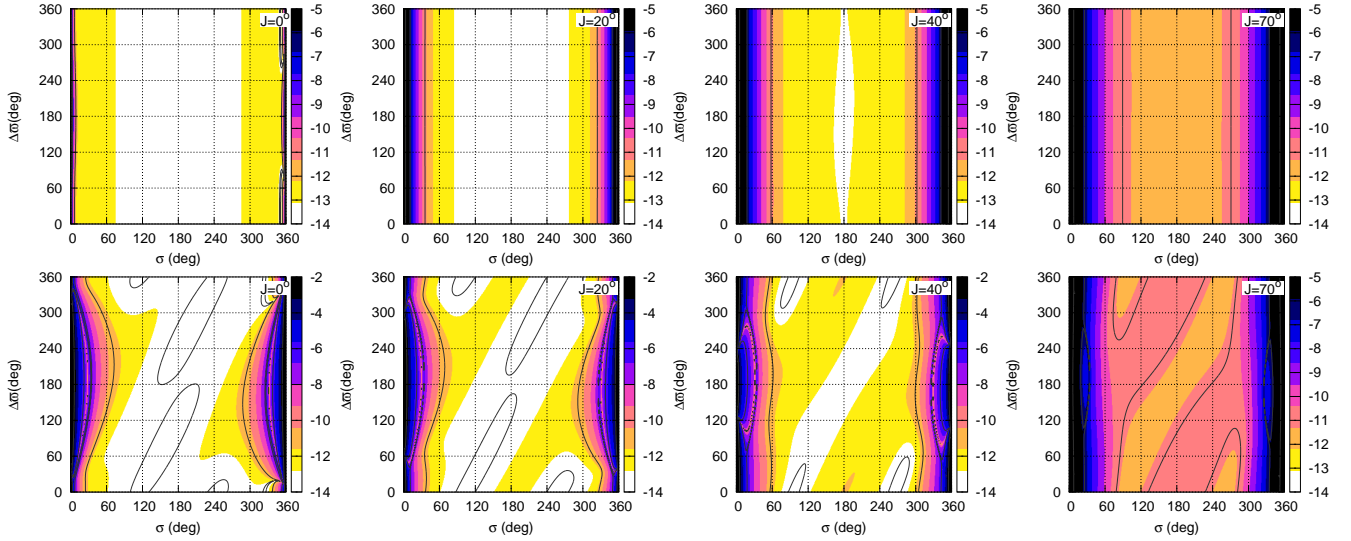


Figure 10. The relative error between the semianalytical averaged Hamiltonian, $\bar{\mathcal{H}}$, and the analytical expansion, \mathcal{H}_2 . We consider two Jupiter-like planets at 1 au with $e_i = 0.01$ (top row), and $e_i = 0.15$ (bottom row). White regions are the most adequate to moderate the dynamics using the \mathcal{H}_2 model.

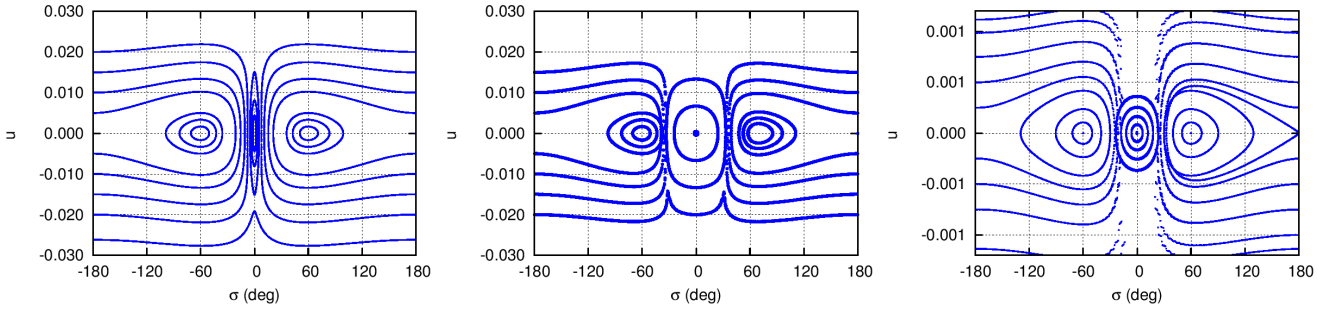


Figure 11. The phase space described by the semianalytical model $\bar{\mathcal{H}}$ in the plane (u, σ) for same initial conditions than Fig. 2. Left panel. Jupiter pair planets in quasi-circular orbits ($e_i = 0.01$). Middle panel. Jupiter pair planets with moderate eccentricities ($e_i = 0.15$). Right panel. Earth-like planets ($m_i = 3 \times 10^{-6} M_\odot$) in quasi-circular orbits.

the secular resonance Lidov-Kozai (LK) provides conditions for periodic orbits for inclined systems, and its centre of libration is located at $\omega = \pm 90^\circ$ (e.g. Lidov 1961; Kozai 1962; Kinoshita & Nakai 2007). The secular Hamiltonian of RTBP (expanded up to quadrupole order in the semi-major axis ratio a_1/a_2 and averaged with respect to the fast periods λ_1 and λ_2) does not depend on Ω . Hence, its conjugated action is a constant; consequently,

$$\sqrt{\mathcal{G}} m_0 a(1 - e^2) \cos(i) = \text{const} . \quad (22)$$

Evidence of Lidov-Kozai resonance for planetary systems was found in the 2:1 MMR (Antoniadou & Voyatzis 2013) and compared with the circular RTBP. As was pointed by Libert & Tsiganis (2009) the stability of some inclined exoplanetary systems may be associated with the LK resonance. Moreover, Morais & Namouni (2016) showed that the LK resonance is present for retrograde orbits as well as in prograde orbits and plays a key role in coorbital resonance capture for circular RTBP.

The LK resonance occurs in hierarchical planetary systems and can be identified dynamically. The centre of this resonance occurs when the mutual inclination between the bodies and the shape of their orbits remain *frozen* in the in-

tegration. This fact occurs at $\Delta\varpi = \pm 90^\circ$. Thus, we identify the centre of LK resonance throughout different dynamical maps when the amplitude of oscillation for e , J and ω tends to zero.

In our development we average over the sum $\lambda_1 + \lambda_2$ instead of λ_1 , λ_2 , obtaining new conserved quantities. Nonetheless, at the limit when the mass ratio goes to zero ($m_2/m_1 \rightarrow 0$) we recovered the results from RTBP, from conservation of angular momentum (see Eq. 14 and Eq. 22).

The Figure 12 shows the variation of oscillation for e_2 in the plane $(\sigma, \Delta\varpi)$, setting two equal mass planets at low eccentric orbits ($e_1 = e_2 = 0.15$) for several different values of initial mutual inclinations. At the left panel, where $a_1 = a_2$, when initial mutual inclination is low we can identify QS orbits at $(0^\circ, 180^\circ)$, L_4 at $(60^\circ, 60^\circ)$, AL_4 at $(\simeq 70^\circ, \simeq 250^\circ)$. As the initial mutual inclination increases, the regions of periodic orbits shrink being only robust the L_4 condition that survives even for $J = 36^\circ$ (tiny dark region at the bottom panel). We have realized that setting $a_1 = a_2$ does not give any further information about the possible existence of HS neither the Lidov Kozai resonance. Thus, following our results from Section 2 we set $u = 1.2U_3$ ($a_1 = 1.004838$ and $a_2 = 0.99517$), showing the results in the right column of

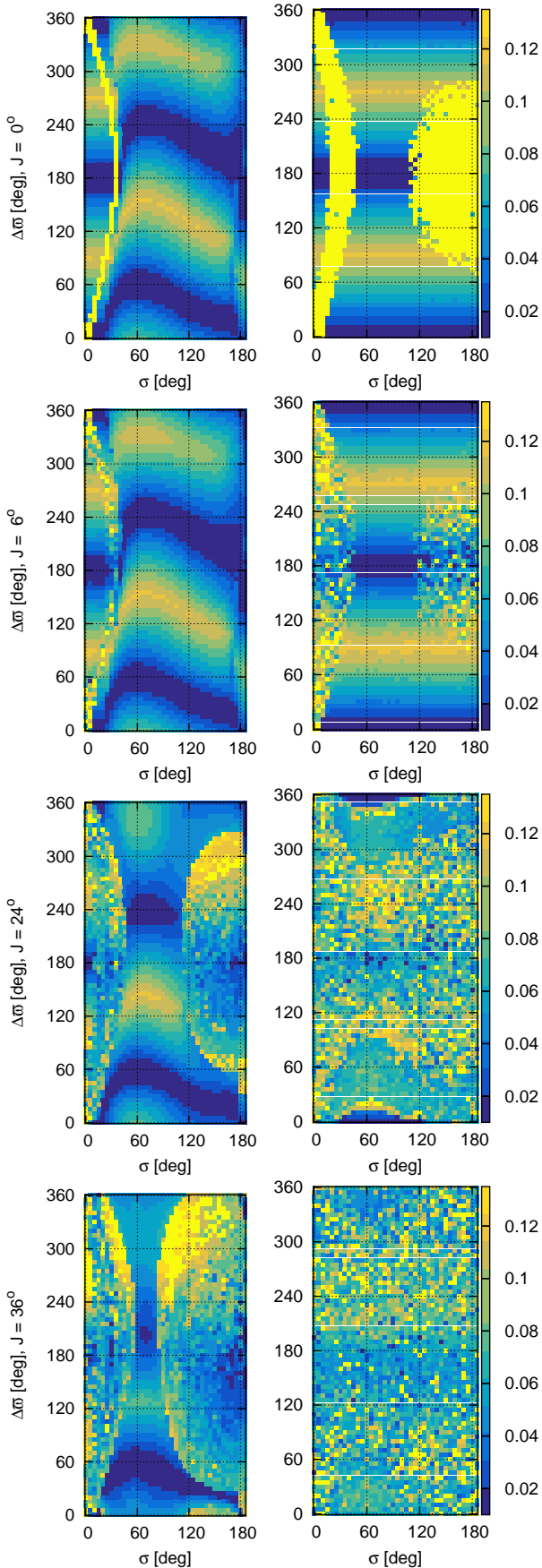


Figure 12. Initial conditions integrated for 10^4 periods with $e_1 = e_2$ and $m_1 = m_2 = 4M_\oplus$. Initial conditions for left column have $a_1 = a_2 = 1$ au, while for right column $a_1=1.004838$ and $a_2=0.99517$ au. Colour scale represents the amplitude variation of e_2 . Each row correspond to a different initial J .

Figure 12. There, the HS region appears at $\Delta\varpi = 0^\circ, 180^\circ$, however it is not present for $J = 0^\circ$ at $(\sigma, \Delta\varpi) = (\simeq 180^\circ, \simeq 180^\circ)^4$.

To optimize the identification of the region where the LK configuration appears, we study the plane (e_1, e_2) and initial conditions with $\omega_2 = 90^\circ$, $\sigma = 180^\circ$, $t_1 = 180^\circ$, $\Delta\varpi = s_1 = s_2 = 0^\circ$, and $u = 1.2U_3$. In this plane we varied J for different mass ratios, ranging from $\log(m_2/m_1) = -3$ to 0. Figure 13 resumes the results with a colour scale proportional to the variation of the mutual inclination, J . We identify two regions of periodic orbits. One region corresponding to $e_1 \simeq e_2$, which is easier to identify for low mutual inclination (see first column, $J = 10^\circ$) and the other one corresponding to $e_1 \simeq 0$ and $e_2 > 0.3$ depending on J and the mass ratio, that we refer as LK region. For a very low mass ratio, $m_2/m_1 \simeq 0.001$ (near RTBP conditions, top row in the figure), it is easy to find the LK resonance in the range of mutual inclination $10^\circ < J < 50^\circ$. This configuration is only found up to $m_2/m_1 \simeq 0.178$ for very high values of e_2 .

In Figure 14 we plot both regions in the parameter space setting $m_2/m_1 \simeq 0.001$. Top and Middle rows shows integrations with the \mathcal{H}_2 model and the N-body code respectively, in the HS region on the plane $(\Delta\varpi, e_2)$. We used the same colours in both panels to facilitate the comparison between them. Evidently, the \mathcal{H}_2 model is limited to small (or even moderate) inclinations and eccentricities, reproducing very well the parameter space with the oscillation centres slightly displaced. We numerically verified that the results are indistinguishable between using $m_2 = 0$ (RTBP) or $m_2/m_1 = 10^{-3}$. Although, the systems are well reproduced for moderate mutual inclinations, the interactions between the bodies are evident for some orbits showing chaotic motion in the N-body integrations.

On the other hand, at the bottom row of Figure 14 we show the LK region on the plane (ω_2, e_2) for the same values of initial J . The results for LK at $J = 18^\circ$ agree with Namouni (1999) for the RTBP inside the 1:1 MMR. The LK region is a mixture of dynamical regimes and it was insightful depicted numerically by Namouni (1999). In Figure 15 we show these different kind of motions in the plane (u, σ) for $J = 18^\circ$ using the same colours and conditions that in bottom right hand-panel of Figure 14. In the region of low eccentricities the motion is of horseshoe-type and ω_2 circulates. Regions at $\omega_2 = 0^\circ$ or 180° , where ω_2 librates with moderate values of e_2 , are those corresponding to passing orbits. We can identify the LK resonance at $\omega_2 = \pm 90^\circ$ with $e_2 \simeq 0.4$ (where ω_2 librates), and near to the LK resonances is the vase-like domain where transitions between $HS - QS$ orbits are present. However, the analytical \mathcal{H}_2 model was not able to reproduce the structure of the phase space. Also, the phase space for $J = 5^\circ$ only shows transition orbits and temporary $HS - QS$ orbits.

To resume the location of the LK resonance, we plot in the plane (e_2, J) the amplitude of oscillation of J , setting $e_1 = 0$ for different mass ratios (see Figure 16). We can perfectly identify that the LK resonance is present up to $J \simeq 50^\circ$ and its appearance strongly depends on the mass ratio.

⁴ Besides, is present for $J = 0^\circ$ with $a_1 = a_2$. Its Megno value shows that is highly chaotic.

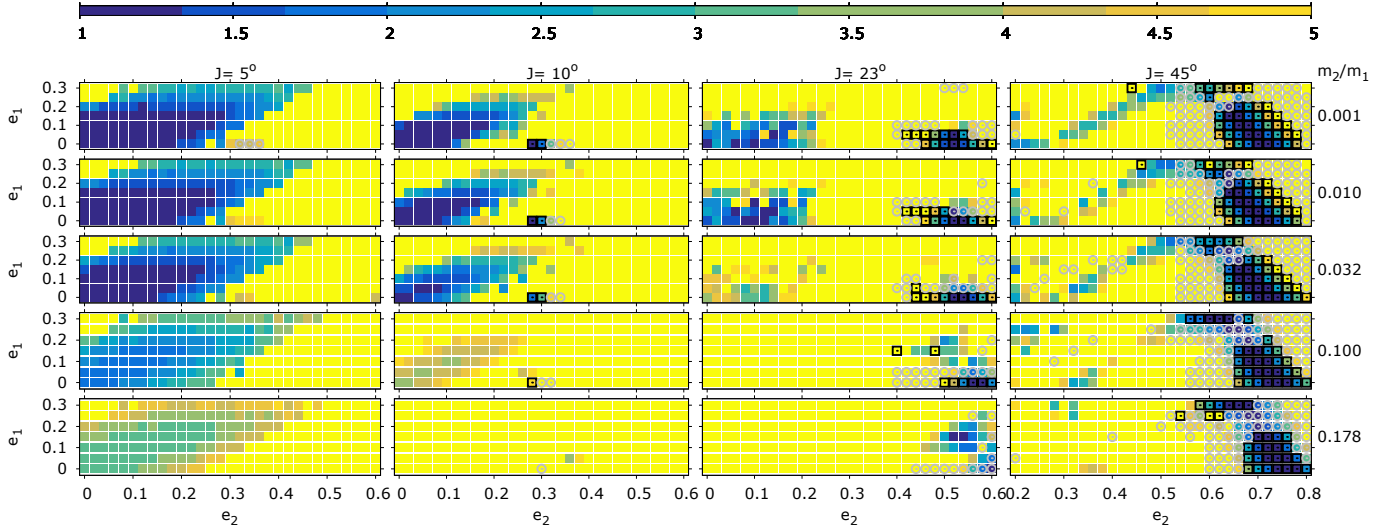


Figure 13. Initial conditions integrated for 10^5 periods. Black squares correspond to amplitude of $\omega_2 < 10^\circ$, grey circles for $10^\circ < \omega_2 < 20^\circ$. For the remaining initial conditions ω_2 circulates very slowly. Colour scale is proportional to the oscillation variation of J .

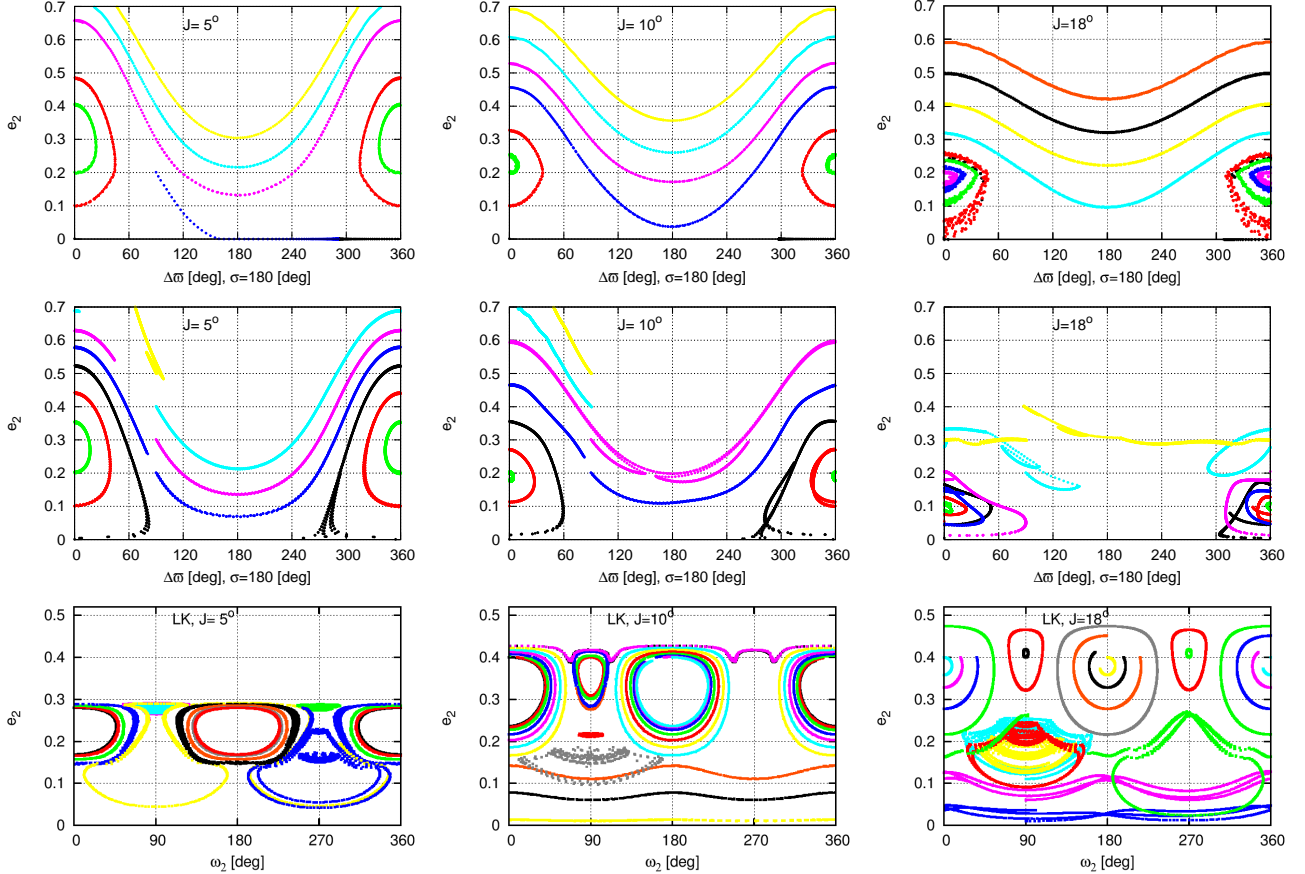


Figure 14. The phase space for a given value of \mathcal{AM} and different initial mutual inclinations ($J = 5^\circ$, $J = 10^\circ$, $J = 18^\circ$ from left to right). First and second row correspond to phase space using \mathcal{H}_2 and N-body integrations for 3×10^5 periods respectively in the plane ($\Delta\omega$, e_2) while the bottom row correspond to integrations on the plane (ω_2 , e_2) with $m_1 = 3 \times 10^{-6} M_\odot$, $m_2 = 3 \times 10^{-9} M_\odot$. Each colour represents the evolution of a different initial condition.

Thus, for example, earth-like planets can be in the centre of the LK resonance at low or high inclinations. In Figure 17 we only plot the points corresponding to the minimum amplitude of oscillation of J for several mass ratios. When $m_2/m_1 \rightarrow 0.3$, the LK resonance almost dissipates and the

strong interactions cause that the amplitude of oscillation for ω_2 increases. However, they are regular orbits, according to their Megno value $\langle Y \rangle (\lesssim 2.02)$.

Contrary to the case of Figure 14, the case of general problem (both planets with similar masses) is slightly dif-

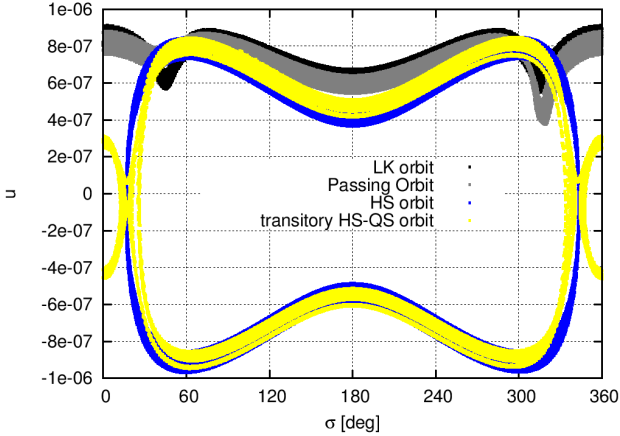


Figure 15. Examples of dynamical regimes present in Figure 14. See text for more detail.

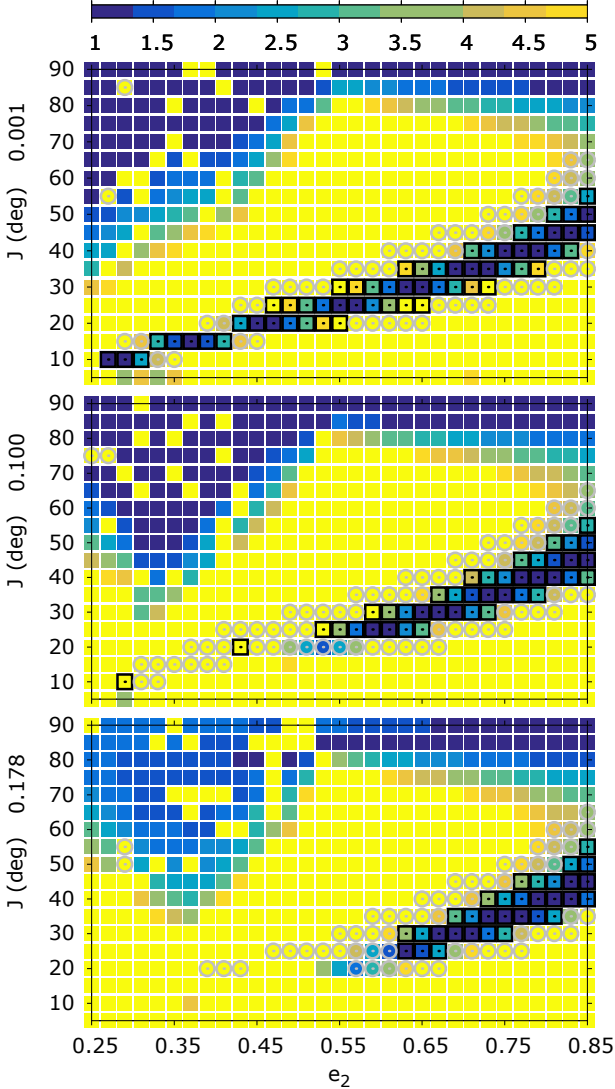


Figure 16. Location of LK resonance centre of depending on mass ratio and initial mutual inclination. The more massive planet is on circular orbit $e_1 = 0$ with remaining orbital elements as in Figure 13. The initial conditions were integrated for 10^5 periods. Black squares correspond to amplitude of $\omega_2 < 10^\circ$, grey circles to $10^\circ < \omega_2 < 20^\circ$. For the remaining initial conditions ω_2 circulates very slowly.

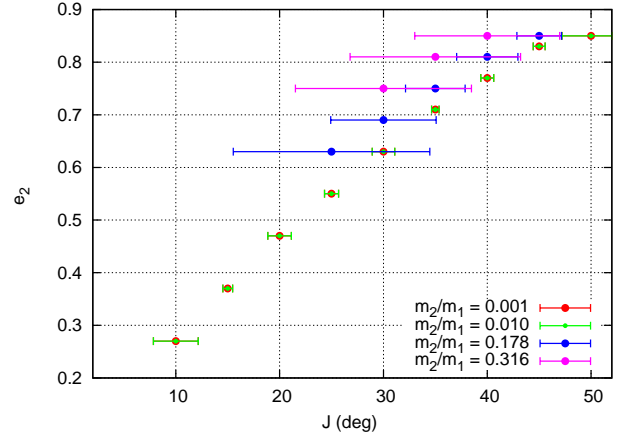


Figure 17. Location of the LK resonance centre depending on the mass ratio and the initial mutual inclination. Error bars are proportional to oscillation of ω_2 .

ferent, and easier to analyse on the plane $(\Delta\varpi, e_2)$. The averaged analytical \mathcal{H}_2 model works well even for high inclinations and we are able to analyse the structure depicted by numerical integrations. The Figure 18 shows the phase space for three different mutual inclinations, J , and moderate eccentricities (initially, $a_1 = a_2 = 1$ ua, $m_1 = m_2 = 3 \times 10^{-6} M_\odot$, and $e_1 = e_2 = 0.2$). When the initial conditions have $\sigma = 60^\circ$ (top row) we can easily identify two islands of stability corresponding to L_4 (at $\Delta\varpi = 60^\circ$) and AL_4 (at $\Delta\varpi \simeq 240^\circ$) configurations. The L_4 region is very well depicted by the model, even for $J = 18^\circ$, but the AL_4 region shifts artificially the centre for $\Delta\varpi \rightarrow 270^\circ$; besides the amplitude of e_2 is well represented. This effect is due to the limitations of expansions. For quasi circular orbits this shift vanished.

In bottom row of Figure 18, when $\sigma = 180^\circ$, we set $u = 1.2U_3$. The oscillation centres are around $\Delta\varpi \simeq 0^\circ$ and $\Delta\varpi \simeq 180^\circ$. Indeed, the central point with $\Delta\varpi \simeq 180^\circ$ may correspond to the Euler configuration L_3 ($J \rightarrow 0^\circ$), which is unstable in the RTBP. When J increases, this family is the only one that survives, although it seems chaotic in this plane. The other centre, around $\Delta\varpi \simeq 0^\circ$, correspond to the family identified as unstable by [Hadjimetriou et al. \(2009\)](#); [Hadjimetriou & Voyatzis \(2011\)](#) in the frame of coplanar planetary problem, using Jupiter planets. For $J \lesssim 20^\circ$ the model perfectly matches N-body integration. After that, this region become unstable. Then, we plot results in the projected plane (σ, u) for $J = 10^\circ$ and $J = 18^\circ$ to show that chaotic orbits in this region corresponds to $HS - QS$ transition orbits (N-body integration with grey points). However, the general behaviour of HS is captured by the \mathcal{H}_2 model.

We tested a wide variety of systems with equal mass planets, from two Earth-mass planets to two Jupiter-mass planets with mutual inclinations as high as 60° in the region previously identify as LK. We not find evidence of LK resonance. For high mutual inclinations, the systems are indeed strongly chaotic, and regular motion is allowed very close to the exact location of L_4 or AL_4 , being the region around L_4 broader.

Also, it is important to remark that as the mutual inclination is greater than 10° , the systems exhibit chaotic behaviour if the initial conditions do not corresponds to the equilibrium solution ($e_1 = e_2$, for $m_1 = m_2 = 1M_\oplus$). Never-

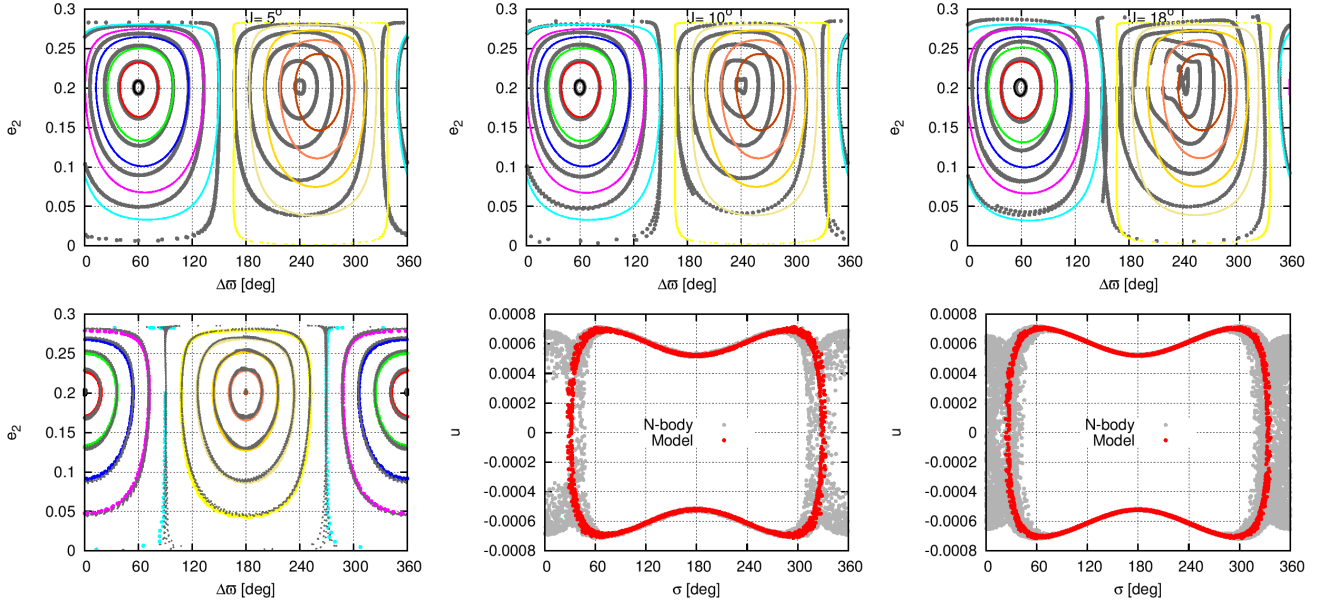


Figure 18. The phase space for a given value of \mathcal{AM} and initial mutual inclination $J = 5^\circ$, $J = 10^\circ$, $J = 18^\circ$ (from left to right respectively). Top row. Two Jupiter-like planets with $a_1 = a_2 = 1$, $\sigma = 60^\circ$ (Lagrangian region). Bottom row. Two planets in the HS region, with mass $3 \times 10^{-6} M_\odot$, $\sigma = 180^\circ$, and $u = 1.2U_3$. We plot with grey dots the N-body integrations, and with colours the \mathcal{H}_2 model integrations.

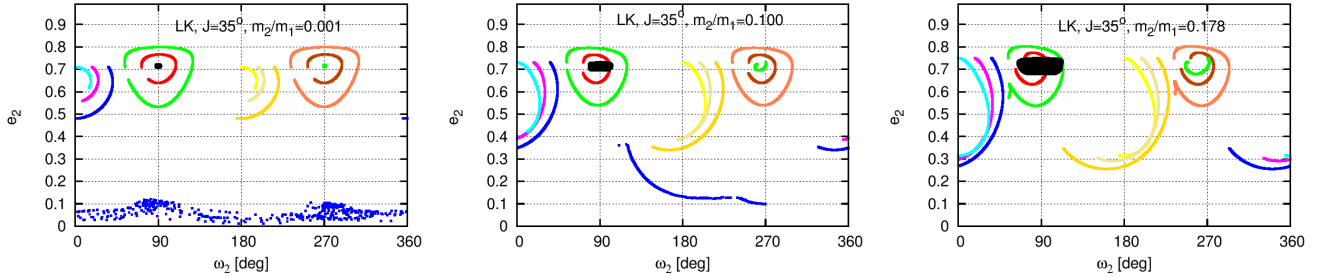


Figure 19. The phase space for a given value of \mathcal{AM} to show the LK resonance centre for $J = 35^\circ$ for three different mass ratios.

theless, we find some systems initially located at high mutual inclinations that can be in coplanar orbits after scattering.

N-body integrations of Figure 19 shows the example of LK phase portraits in the plane (ω_2, e_2) for $J = 35^\circ$ and different mass ratios, with $m_1 = 1M_\oplus$ and $e_1 = 0.001$. Note the centre of LK resonance located at $\omega_2 = \pm 90^\circ$. Low eccentric regime, $e_2 \lesssim 0.2$, is usually chaotic for this value of J . We use different colours to identify the evolution of initial conditions integrated for 3×10^5 periods, while the condition corresponding to $\omega_2 = 90^\circ$ was integrated during 10^7 periods. Is easy to see the importance of the forced oscillation around LK centre when $m_2/m_1 \rightarrow 0.2$, justifying the error bars in the Fig. 17.

Finally we analyse the 3D configurations for periodic orbits mentioned in Figure 1: L_4 , AL_4 , QS , L_3 , U . To construct the families of periodic orbits in the spatial case we began from the previous known results in the planar case and varied the mutual inclinations, J . For each family we checked that $\dot{\sigma} = \Delta \dot{\omega} = 0$, setting the remaining angles equal to zero. We believe that, this is a natural extension from the periodic orbits in the equal-mass planar case, although a more

rigorous search should use the local extrema of the semianalytical Hamiltonian. The top panel in Figure 20 shows the variation of amplitude of oscillation for e_2 , Δe_2 , for systems with different initial mutual inclinations and integrated during 10^6 periods. For L_4 , AL_4 , and QS orbits we set initial semi major axes $a_i = 1$ ua, while for L_3 and U we set a_i using $u = 1.2U_3$. We calculate the Megno value for every orbit, $\langle Y \rangle$, but we choose to show Δe_2 indicator because is easier to see the smooth *degradation* of orbits as J increases; alternatively ΔJ is a good indicator too. The most regular orbits are those corresponding to L_4 configurations (even for $J \simeq 60^\circ$). AL_4 orbits are regular when $J \lesssim 38^\circ$ and QS orbits are regular up to $J \lesssim 28^\circ$. On the other hand, U -type configurations remain stable and bounded for choosen planetary masses ($4 M_\oplus$) when $J \lesssim 20^\circ$, although the evolution of orbital elements shows a slow chaos diffusion. The L_3 orbits are also interesting. For $J = 0$ the orbits are unstable, yielding to close encounters between the planets, however for $J > 0$ the orbits become stable for at least 10^6 periods ($\langle Y \rangle > 5$). Even for $J \simeq 60^\circ$ the orbits oscillate around

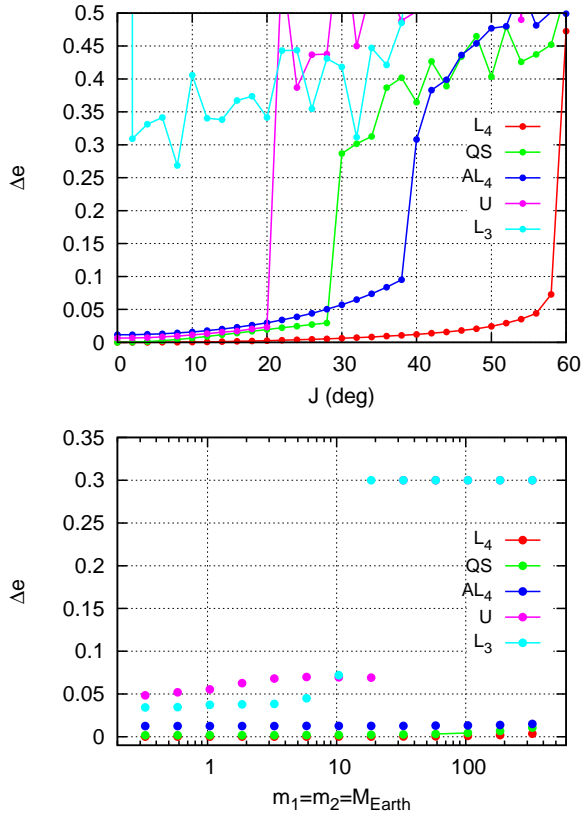


Figure 20. Analysis of periodic orbits L_4 , AL_4 , QS , L_3 , U in the non-coplanar case using as indicator the variation of Δe_2 . Results correspond to N-body integrations for 10^6 periods. Top panel. Results considering two planets with masses $m_1 = m_2 = 4M_\oplus$, and $e_i = 0.15$. The smooth variation of Δe_2 , when we increase J , is a good indicator of regular orbits ($\langle Y \rangle \approx 2$), although almost all the orbits survives at least for 10^6 periods. Bottom panel. Analysis of stability for inclined systems depending on their masses (see text for more detail).

$\Delta\varpi = 180^\circ$, although when $0^\circ < J < 20^\circ$ their chaoticity is more bounded.

The bottom panel of Fig. 20 shows Δe_2 , attained during the integrations, for several mass values of pair of planets. We choose to show $J = 5^\circ$ to illustrate the general behaviour of the families. L_4 , AL_4 , and QS configurations are regular and robust configurations in the range $0.3M_\oplus < m_i < 1M_{Jup}$. The U -type orbits seems to be regular for masses $m_i \lesssim 10m_\oplus$, despite long-term diffusion is observed and they remain in this configuration at least for 1 Gy; in contrast for systems with more massive planets ($m_i \gtrsim 20m_\oplus$) close encounters causes expulsion of one planet ($a_i > 2$ au) in less than 10^4 periods. This same limit was observed for the coplanar case. The L_3 configurations are chaotic but bounded for $m_i \lesssim 15M_\oplus$ and, also like U configurations, after this value of masses the systems are quickly destroyed.

5 CONCLUSIONS

We studied the three-body problem in the context of coorbital resonance, considering coplanar and spacial configurations. We followed several approaches: analytical (\mathcal{H}), averaged analytical (\mathcal{H}_2 , Eqs. 9), and semi-analytical ($\tilde{\mathcal{H}}$, Eqs.

20). We found appropriate angles and actions (Eqs. 14) that evidence the conserved quantities, verifying the results with N-body integrations. Some tests were carried out in the limit of the RTBP.

We analysed the orbital evolution using the different models, and identified the regular and chaotic region in the plane (σ, u) for massive planets. In fact, the phase space structure given by the integrable approximation \mathcal{H}_{00} is not adequate for any condition, and our semianalytical model is more accurate (see Fig. 2). We roughly established a mass limit for the existence of Horseshoe orbits when working with two massive planets depending on the eccentricities and mutual inclinations (see Fig. 4).

The analytical \mathcal{H}_2 model described correctly the resonant motion up to moderate eccentricities ($e_i \leq 0.3$) and initial mutual inclinations ($J \leq 35^\circ$). It always happens outside the region associated with QS motion. Using the \mathcal{H}_2 model, we speeded the orbital evolution by a factor of ~ 50 . However, depending on the particular problem, the secular frequencies are overestimated (even 10 times in our examples). Thus, when working with dissipative forces as tides, Yarkovsky or YORP, the secular effects should be scaled properly in each case.

The analytical \mathcal{H}_2 model was accurate in the case of the general-three body problem with high mutual inclinations, while in the context of the RTBP the semianalytical model $\tilde{\mathcal{H}}$ or N-body integrations should be used.

We established the location of Lidov-Kozai resonance within the 1:1 MMR. The location of LK resonance centre strongly depends on the mass ratio and on the mutual inclination. The limit for the existence starts from the case of RTBP until $m_2/m_1 \lesssim 0.3$, despite planets with comparable masses force the excitation of the orbits around the equilibrium solution.

Thus, when we considered inclined pair of planetary systems, L_4 , AL_4 and QS orbits are the most regulars, and we discover some interesting and very unexpected results for U and L_3 orbits. The identified unstable orbits U by Hadjidemetriou et al. (2009) are, in fact, regular and very stable orbits for pair of Earth-like planets up to mutual inclinations lower than 20° . In the case of inclined systems, contrary to the planar problem, the L_3 orbits are very chaotic but bounded. We checked that for $J \lesssim 30^\circ$ the orbits remain stable at least for 50 My.

The models developed here can be used for a systematic study of the secular dynamics in the coorbital regime with the Solar System planets, and also, with exoplanetary systems. Further work is necessary to study the families of periodic orbits (and stationary solutions). Moreover, it is necessary further work to characterize the change in the phase space-structure of 1:1 MMR and to give rigorous definitions for the families of periodic orbits in the spatial case and their relationship with planar and also with the restricted case.

REFERENCES

- Antoniadou K. I., Voyatzis G., 2013, *Celestial Mechanics and Dynamical Astronomy*, **115**, 161
- Beaugé C., Michtchenko T. A., 2003, *MNRAS*, **341**, 760
- Brouwer D., Clemence G. M., 1961, *Methods of celestial mechanics*. Academic Press, New York
- Carpino M., Milani A., Nobili A. M., 1987, *A&A*, **181**, 182
- Cincotta P. M., Simó C., 2000, *A&AS*, **147**, 205

- Dobrovolskis A. R., 2013, *Icarus*, **226**, 1635
- Ferraz-Mello S., ed. 2007, Canonical Perturbation Theories - Degenerate Systems and Resonance Astrophysics and Space Science Library Vol. 345
- Ford E. B., Gaudi B. S., 2006, *ApJ*, **652**, L137
- Ford E. B., Holman M. J., 2007, *ApJ*, **664**, L51
- Giuppone C. A., Beaugé C., Michtchenko T. A., Ferraz-Mello S., 2010, *MNRAS*, **407**, 390
- Giuppone C. A., Morais M. H. M., Boué G., Correia A. C. M., 2012, *A&A*, **541**, A151
- Hadjidemetriou J. D., Voyatzis G., 2011, *Celestial Mechanics and Dynamical Astronomy*, **111**, 179
- Hadjidemetriou J. D., Psychoyos D., Voyatzis G., 2009, *Celestial Mechanics and Dynamical Astronomy*, **104**, 23
- Haghighipour N., Capen S., Hinse T. C., 2013, *Celestial Mechanics and Dynamical Astronomy*, **117**, 75
- Kinoshita H., Nakai H., 2007, *Celestial Mechanics and Dynamical Astronomy*, **98**, 67
- Kozai Y., 1962, *AJ*, **67**, 591
- Laskar J., 1990, *Icarus*, **88**, 266
- Laskar J., Robutel P., 1995, *Celestial Mechanics and Dynamical Astronomy*, **62**, 193
- Laughlin G., Chambers J. E., 2002, *AJ*, **124**, 592
- Leleu A., Robutel P., Correia A. C. M., 2015, *A&A*, **581**, A128
- Libert A.-S., Tsiganis K., 2009, *A&A*, **493**, 677
- Lidov M. L., 1961, *Iskus. sputniky Zemly* (in Russian), **8**, 5
- Mikkola S., Innanen K., Wiegert P., Connors M., Brasser R., 2006, *MNRAS*, **369**, 15
- Morais M. H. M., Namouni F., 2016, preprint, ([arXiv:1602.04755](https://arxiv.org/abs/1602.04755))
- Moulton F. R., 1914, *An introduction to celestial mechanics*. New York, The Macmillan company
- Namouni F., 1999, *Icarus*, **137**, 293
- Páez R. I., Efthymiopoulos C., 2015, *Celestial Mechanics and Dynamical Astronomy*, **121**, 139
- Robutel P., Pousse A., 2013, *Celestial Mechanics and Dynamical Astronomy*, **117**, 17
- Robutel P., Niederman L., Pousse A., 2015, preprint, ([arXiv:1506.02870](https://arxiv.org/abs/1506.02870))
- Sidorenko V. V., Neishtadt A. I., Artemyev A. V., Zelenyi L. M., 2014, *Celestial Mechanics and Dynamical Astronomy*, **120**, 131
- Vokrouhlický D., Nesvorný D., 2014, *ApJ*, **791**, 6
- Voyatzis G., Antoniadou K. I., Tsiganis K., 2014, *Celestial Mechanics and Dynamical Astronomy*, **119**, 221

ACKNOWLEDGEMENTS

The authors wish to thank Dr. Beaugé for his stimulating suggestions and to Dr. A. L. Serra for her valuable comments. We acknowledge financial support from CONICET/FAPERJ (39593/133325). The numerical simulations have been performed on the local computing resources at the Córdoba University (Argentina).

This paper has been typeset from a $\text{\TeX}/\text{\LaTeX}$ file prepared by the author.